*Journal of Applied Fluid Mechanics*, Vol. 19, No. 1, pp. 3268-3279, 2026. Available online at <a href="https://doi.org/10.47176/jafm.19.1.3616">www.jafmonline.net</a>, ISSN 1735-3572, EISSN 1735-3645. <a href="https://doi.org/10.47176/jafm.19.1.3616">https://doi.org/10.47176/jafm.19.1.3616</a>



# Variation Law and Calculation Model of Slurry Critical Non-silting Velocity under the Action of Swirler

S. Zhao<sup>1,2</sup>, J. Bao<sup>2†</sup>, J. Ji<sup>1</sup>, X. Zhang<sup>1</sup>, Y. Ma<sup>1</sup>, Y. Yin<sup>2</sup>, and Y. Liu<sup>3</sup>

School of Intelligent Manufacturing, Jiangsu Vocational Institute of Architectural Technology, Xuzhou 221116, China
 School of Mechatronic Engineering, China University of Mining and Technology, Xuzhou 221116, China
 CCTEG Chongqing Research Institute, Chongqing 400039, China

†Corresponding Author Email: <a href="mailto:cumtbjs@cumt.edu.cn">cumtbjs@cumt.edu.cn</a>

### **ABSTRACT**

Critical non-silting velocity, a key parameter in slurry pipeline transport systems, significantly influences operational conditions and economic viability. A lower critical non-silting velocity is advantageous for reducing energy consumption, minimizing pipeline wear, and enhancing system stability. To achieve this objective, this study proposes a method to improve the particle suspension state within slurry pipelines through the addition of a swirler. The research comprehensively investigated variations in the critical non-silting velocity under diverse conveying conditions, comparing scenarios both with and without the swirler. The results demonstrate that the swirler induces a circumferential flow within the pipeline. This flow exerts a drag force on particles, promoting their transition from a settled state to a non-silting flow regime, thereby reducing the critical non-silting velocity. For slurries characterized by low concentration, small particle size, and low density, the circumferential kinetic energy required to alter their flow state is smaller; consequently, the reduction in critical non-silting velocity is more pronounced. The calculation model of critical non-silting velocity considering the swirl characteristics was established. Compared to experimental values, the model yields an average error of 9.10% and a maximum error of 14.08%.

### Article History

Received April 19, 2025 Revised July 18, 2025 Accepted August 7, 2025 Available online November 5, 2025

### Keywords:

Pipeline transportation Particle settling Swirler Critical non-silting velocity Calculation model

### 1. Introduction

With the gradual depletion of shallow coal resources (Zhang et al., 2023), the extraction of deep-earth minerals has emerged as an inevitable global trend, particularly in China (Chen et al., 2023). To address the challenges of deep resource exploitation, Xie et al. (2017a, 2017b, 2018, 2019) pioneered a transformative technical framework: insitu fluidized mining of deep coal. This approach integrates unmanned, intelligent shield operations for underground coal extraction with the conversion of coal into transportable fluidized media-including liquefied, gasified, electrochemical, and biological forms-for subsequent surface delivery.

For ultra-deep mines, conventional wire-rope hoisting systems prove economically and operationally inadequate to meet the demands of fluidized coal transport (Singh, et al. 2016; Wang, et al. 2019; Galy & Giraud, 2023). Given the inherent advantages of pipeline hydraulic conveyance-superior continuity, efficiency, and controllability (Das, et al. 2020, 2021) this technology represents a viable solution

for post-fluidization coal transport. Recently, our research group proposed a deep coal fluidization pipeline lifting system (Bao, et al. 2022), wherein fluidized coal slurry, pressurized through multiple stages, replaces skip-hoist transport and is pumped directly to the surface.

Current research on pipeline transport predominantly focuses on fine-particle slurries (Ma, et al. 2017). However, reduced particle sizes substantially increase slurry preparation and dewatering costs. Post-dewatering challenges include excessively fine particles that exacerbate dust pollution and complicate material handling (Li, et al. 2021). Consequently, increasing coal particle diameter represents a critical development pathway for pipeline technology (Li, et al. 2021), particularly in regions with limited infrastructure and harsh operating environments.

While the deep coal fluidization pipeline lifting system operates primarily in vertical orientation, its design necessarily incorporates horizontal sections. In such configurations, larger particles tend to settle under gravity,

NOMENCLATURE					
$\alpha_{ m l}$	volume fraction of the fluid	$\vec{u}_i$	particle <i>i</i> velocity vector		
$ ho_{ m l}$	fluid density	$m_i$	mass of the particle <i>i</i>		
$u_1$	fluid velocity	$U_{ m C}$	critical non-silting velocity		
$ec{u}_l$	fluid velocity vector	$C_{ m V}$	volume concentration		
$\nabla$	horizontal and vertical gradient operator	$d_{ m s}$	particle diameter		
$\mu_{\mathrm{l}}$	fluid viscosity	$ ho_{ extsf{s}}$	particle density		
$\vec{S}_l$	source term of momentum exchange	D	pipeline inner diameter		
- 1	between fluid and particle				
$\vec{F}_d$	solid-liquid interaction force	S	swirl intensity		
$\alpha_{\rm p}$	particle volume fraction	$S_0$	initial swirl intensity		
$V_{\rm cell}$	fluid computing unit	β	decay rate of swirl intensity		
$V_{p}^{(i)}$	volume of particle <i>i</i> in the cell	$\chi(Z_{\mathrm{sd}})$	spiral flow attenuation function		
$n_{\rm p}$	number of particles in a cell	$Z_{ m sd}$	distance from the outlet of the swirler		
$\vec{F}_{ ext{KTGF}}$	particle fluid dynamics used in the DDPM				
- KIGI	model to consider the interaction between				
	particles (such as particle collision,				
	translation, etc.)				

creating heterogeneous slurry concentration distributions.

This stratification elevates frictional losses during transport (Singh, et al. 2019) and may precipitate pipeline blockage in severe instances.

Swirlers can induce spiral flow fields within pipelines, thereby modifying particle dynamics. Although spiral flow attenuation limits their effectiveness in long-distance surface conveyance, it presents a viable solution for managing short horizontal segments within deep coal fluidization lifting systems (Sun, et al. 2012).

In the 1990s, researchers from Taiyuan University of Technology's Department of Hydraulics pioneered the application of pipe-generated helical flow to sediment transport (Zhao, 2024). Subsequent research by domestic and international scholars has significantly advanced this field. Zhou et al. (2016) developed a side-inlet guide vane swirl generator, demonstrating that both medium-swirl configurations at low mean velocities and weak-swirl regimes at high velocities enhance stability in pneumatic lump-coal conveyance. Li et al. (2021) investigated guide vane angle effects on velocity distributions during spiralflow transport of barreled materials. They determined that increased installation angles generate higher circumferential velocities while promoting more uniform axial flow profiles. In a separate study, Zhou et al. (2016) positioned twisted tapes upstream of pipe elbows to induce spiral airflow. Their results revealed that reduced twist ratios and proximity to elbows significantly improved wear mitigation. Most recently, Zhao et al. (2023) installed guide-vane swirlers upstream of coal slurry pipelines. Their comprehensive analysis quantified elbow wear reduction mechanisms and morphological evolution under swirling flows, establishing a predictive model correlating vane parameters and operational conditions with maximum wear rates, experimentally validating the elbow protection efficacy.

The critical non-silting velocity, defining the minimum operational velocity for slurry pipelines, constitutes a fundamental design parameter in hydraulic conveying systems. Accurate determination of this velocity is essential for successful pipeline operation.

Durand (1952) first established a computational model for the transition velocity at which particles shift from suspension to bedload motion (sliding or rolling along the pipe bottom). Subsequent refinements by Shook and Wasp enhanced this model by correlating the Froude number with slurry concentration and relating the hydraulic gradient to critical velocity.

Current research on the critical non-silting velocity mainly focuses on the axial flow field of the pipeline. The influence law of the spiral flow field generated by the swirler on the critical non-silting velocity is still unclear. Revealing the variation of slurry critical non-silting velocity in swirler-induced spiral flow fields and establishing a predictive model provides crucial theoretical foundations for enhancing the safety and economic viability of deep coal fluidization pipeline lifting systems.

### 2. METHOD

### 2.1 Numerical Simulation Model

Given the transport characteristics of the target slurry, a guide vane swirler, which features high structural strength, low energy consumption, and an unrestricted installation position, has been selected as the research subject (Zhao, et al. 2024). Modification of its structural parameters directly modulates spiral flow characteristics within the pipeline (Saad & Baria, 2014; Baria & Saad, 2013; Kim, et al. 2023), subsequently governing particle transport dynamics and ultimately determining pipeline system performance (Bao, et al. 2025).

The internal flow field of the simulation model was divided by tetrahedral meshes, and the Element Quality and Element Quality of the grid are both above 0.8, as shown in Fig. 1 (Singh, et al. 2020).

The Euler-Lagrange method was used for the numerical simulation of solid-liquid two-phase flow in pipelines, and the fluid control equations are shown below (Li, et al. 2024):

(1) Continuous phase equations

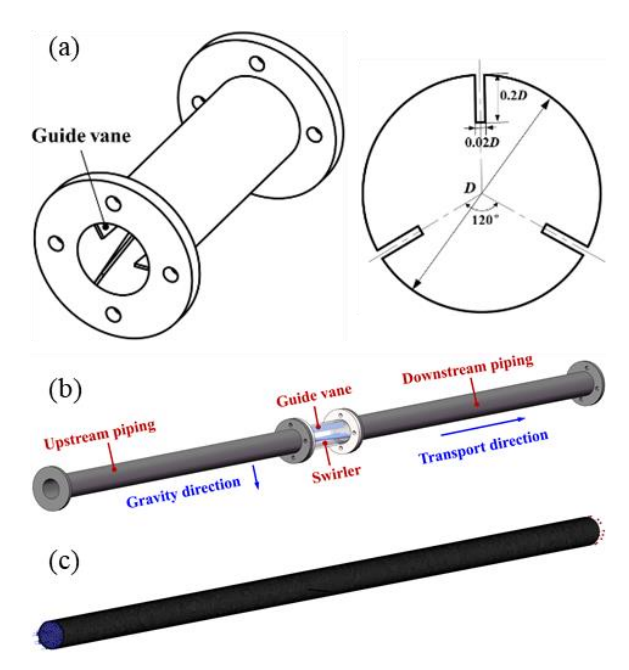


Fig. 1 Structure diagram of the guide vane swirler (a), physical model of transport pipeline (b), and Internal flow field meshing (c)

$$\frac{\partial}{\partial t}(\alpha_l \rho_l) + \nabla \cdot (\alpha_l \rho_l u_l) = 0 \tag{1}$$

(2) Momentum equation

$$\begin{split} &\frac{\partial \left(\alpha_{l} \rho_{l} \overset{\Gamma}{u_{l}}\right)}{\partial t} + \left(\nabla \cdot \alpha_{l} \rho_{l} \overset{\Gamma}{u_{l}} \overset{\Gamma}{u_{l}}\right) = \alpha_{l} \rho_{l} g \times \\ &\nabla \left[\alpha_{l} \mu_{l} \left(\nabla \overset{\Gamma}{u_{l}} + \nabla \overset{\Gamma}{u_{l}}\right)\right] - \alpha_{l} \nabla \overset{\Gamma}{p} + \overset{\Gamma}{S_{l}} \end{split} \tag{2}$$

(3) Momentum coupling

$$\vec{S}_{I} = \frac{1}{V_{cell}} \sum_{i=1}^{n_{p}} \vec{F}_{d} \tag{3}$$

(4) Fluid volume fraction

$$\alpha_{l} = 1 - \alpha_{p} = 1 - \frac{1}{V_{coll}} \sum_{i=1}^{n_{p}} V_{p}^{(i)}$$
(4)

where,  $\alpha_l$  is the volume fraction of the fluid.  $\rho_l$  is the fluid density.  $u_l$  is fluid velocity.  $\vec{u}_l$  is the fluid velocity vector.  $\nabla$  is the horizontal and vertical gradient operator.  $\mu_l$  is the fluid viscosity.  $\vec{S}_l$  is the source term of momentum exchange between fluid and particle.  $\vec{F}_d$  is solid-liquid interaction force.  $\alpha_p$  is the particle volume fraction.  $V_{\text{cell}}$  is a fluid computing unit.  $V_p^{(i)}$  is the volume of particle i in the cell.  $n_p$  is the number of particles in a cell.

### (5) Particle motion equation

Based on the Euler-Lagrange method, the DDPM model is selected to solve the motion law of the particle phase in the pipeline. To overcome the limitation of the discrete phase volume fraction, based on Newton's second law of motion, the motion model equation for solid particles can be expressed as follows:

$$m_{i} \frac{d\overline{u}_{i}}{dt} = m_{i} \frac{\rho_{1}}{\rho_{s}} \overline{u}_{l} \nabla \overline{u}_{l} + m_{i} \frac{3C_{D}}{4} \frac{|\overline{u}_{i} - \overline{u}_{l}|}{d_{s}} \times (u_{i} - u_{l}) + \frac{m_{i} g(\rho_{s} - \rho_{1})}{\rho_{s}} + \overline{F}_{KTGF}^{T}$$

$$(5)$$

where,  $m_i$  is the mass of the particle i.  $\vec{u}_i$  is the particle i velocity vector.  $\rho_s$  is the particle density.  $d_s$  is the particle diameter.  $C_D$  is the drag coefficient.  $\vec{F}KTGF$  is the particle fluid dynamics used in the DDPM model to consider the interaction between particles (such as particle collision, translation, etc.). On the right side of Eq. (5), the first term is the pressure gradient force, the second term is the drag force of the fluid on the particles, and the third term is the buoyancy force of the particles.

### 2.2 Pipeline Transport Test Equipment

To verify the swirler's impact on slurry transport process, this paper selects the critical non-silting velocity as an evaluation metric, and constructs the experimental setup shown in Fig. 2.

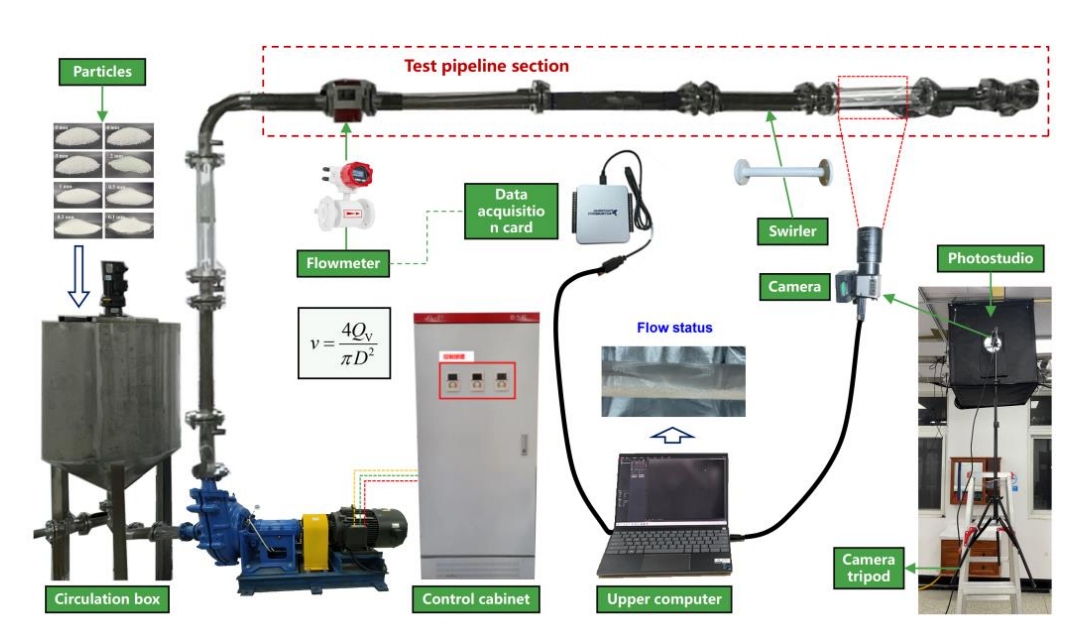


Fig. 2 Critical non-silting velocity test device

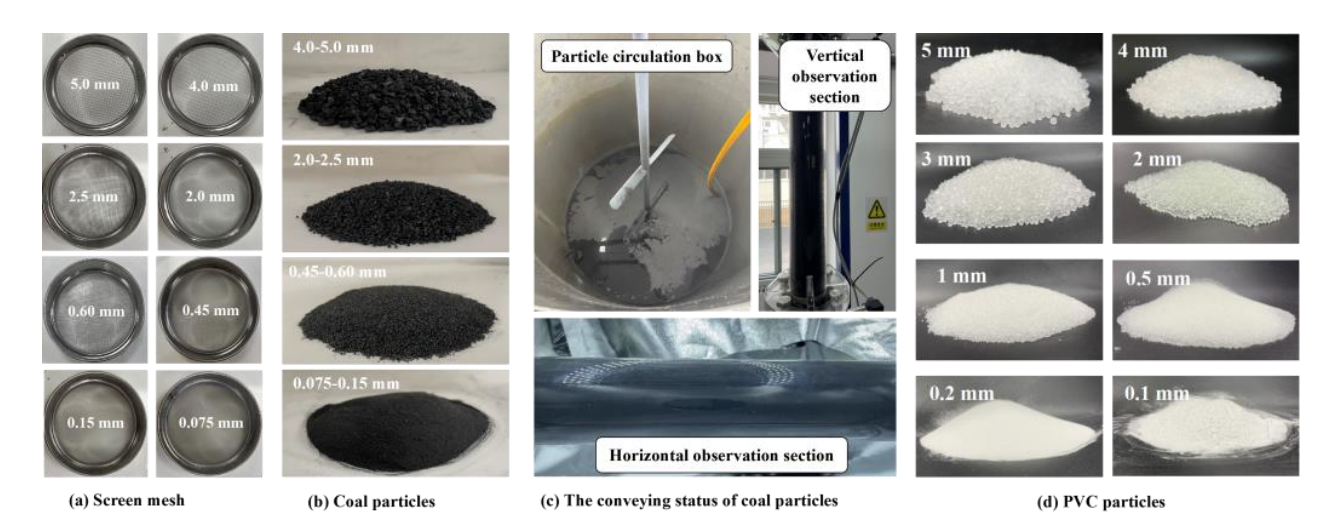


Fig. 3 Real coal particle conveying test

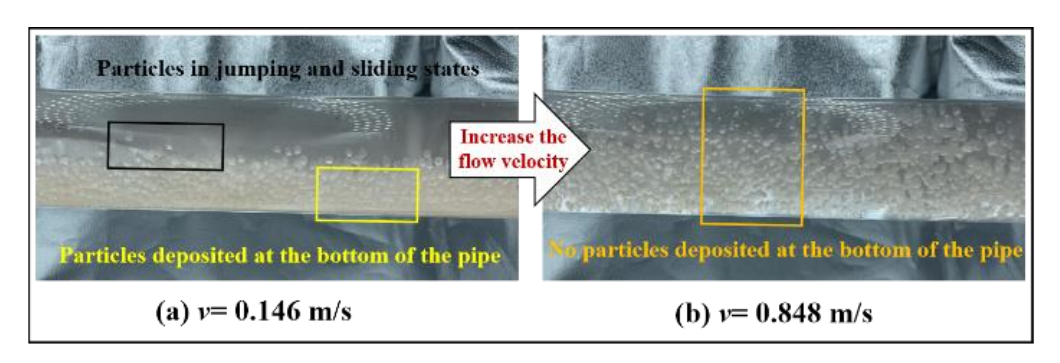


Fig. 4 Critical non-silting velocity detection method

In the experiment, it was found that the actual coal particles as shown in Fig. 3(b) would contaminate the pipeline during transportation, which was not conducive to the camera capturing the transportation state of the particles in the pipeline and was not conducive to observing the critical non-silting velocity, as shown in Fig. 3(c). Therefore, in this paper, PVC particles with a density similar to that of coal and not contaminating the pipeline were customized to replace the coal particles for the experiment, as shown in Fig. 3(d). The test particles were screened and filtered using the sieve shown in Fig. 3(a), and their ratio to water was adjusted to prepare slurries of different concentrations, densities, and diameters.

The swirler was custom-made using 3D printing technology. The critical non-silting velocity - defined as the minimum flow velocity initiating motion of all deposited particles at the pipe bottom - was measured using a WP-UT130/M high-speed industrial camera through the transparent pipeline section. In this experiment, the "Visual Observation Method" was adopted to measure the critical non-silting velocity (Gao, et al. 2016). Specifically, the flow velocity of the pump was adjusted from low to high via a PLC (Programmable Logic Controller). When the flow velocity reached 0.146 m/s, some particles deposited at the pipeline bottom began to move in a suspended state within the pipe, as shown in Fig. 4(a). As the flow velocity increased, the number of suspended particles grew, though partial particles still deposited at the pipeline bottom. When the flow velocity

further increased to 0.848 m/s, all particles stationary at the pipeline bottom started to move forward, as shown in Fig. 4(b). This paper defines the transport velocity corresponding to the particle state shown in Fig. 4(b) as the critical non-deposition velocity. Each working condition was tested 5 times during the experiment, and the average value of all results was taken as the final result.

Table 1 Parameters of test equipment

Equipment name	Parameters	Value
C1	Head (m)	63
Slurry pump	Flow (m <sup>3</sup> /h)	50
Pressure sensor	Measuring range (kPa)	0–10
Flow sensor	Measuring range (m/s)	0–7
High ground	Frame rate	1280×1024
High-speed industrial camera	Resolution ratio (fps)	210

### 3. RESULTS

To master the variation of slurry critical non-silting velocity under the action of the swirler, the motion of particles in the conveying pipeline under the action of the swirler was studied by simulation test, and then the critical non-silting velocity test under different conveying conditions was carried out by simulation test bench.

## 3.1 Particle Settlement in Conveying Pipeline with and Without a Swirler

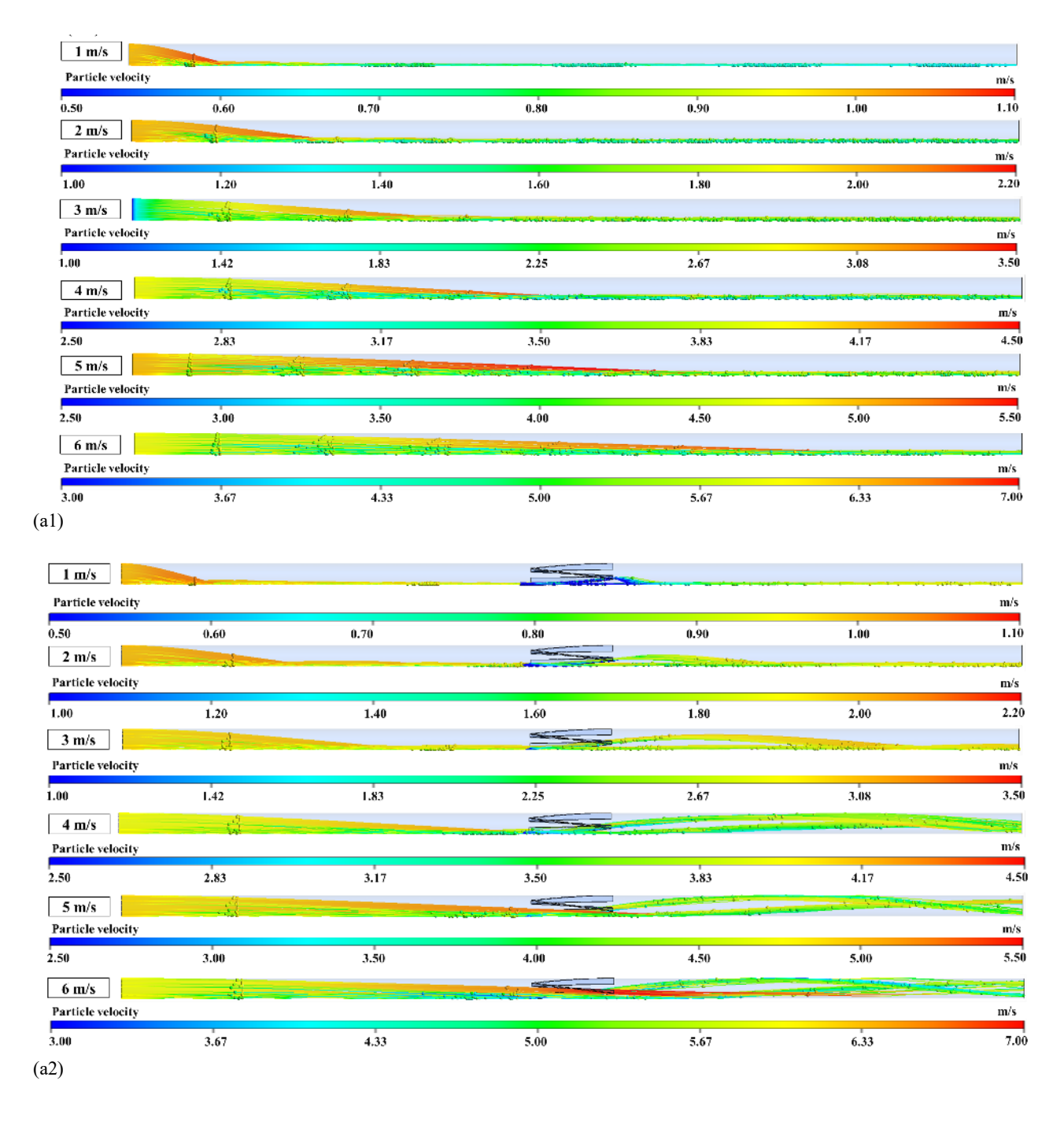
To investigate swirler-induced modifications in transport behavior of large, sedimentation-prone particles, simulations were performed for 5-mm coal particles in horizontal pipelines (Fig. 5). Fig. 5(a1) demonstrates that without swirlers, particles progressively settle along the pipeline under all conveying velocities, and then move forward along the bottom of the pipeline. Lower conveying velocities accelerate this gravitational settling, which also corresponds to the proportion of large particles in the outlet cross-section of the pipe in Fig. 5(b1).

As illustrated in Fig. 5(a2), the incorporation of the swirler results in distinct variations in the movement patterns of large particles advancing along the pipeline bottom under different conveying velocities. At low conveying velocities (v=1 m/s), large particles exhibit a

slight upward trajectory upon passing through the swirler, yet they rapidly settle back to the pipeline bottom shortly thereafter. With increasing conveying velocity, the duration of the upward movement induced in large particles after passing through the swirler is prolonged. Notably, when the conveying velocity reaches or exceeds 4 m/s, large particles adopt a spiraling forward motion in the downstream region of the swirler - a behavior that aligns with the distribution proportion of large particles observed in the outlet cross-section of the pipeline as presented in Fig. 5(b2).

### 3.2 Variation of Critical Non-silting Velocity of Slurry under the Action of a Swirler

Slurry concentration, particle diameter, particle density, and pipe inner diameter have significant effects on the critical non-silting flow velocity. Previous studies



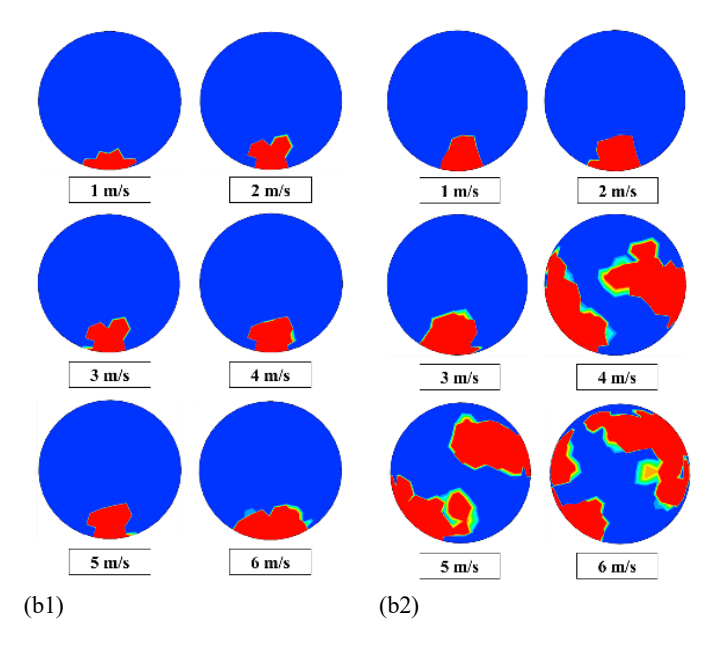


Fig. 5 Particle movement and distribution. a1-b1 are the particle motion state in the pipeline without a swirler and the distribution proportion of pipeline cross-section, respectively; a2-b2 are the particle motion state in the pipeline with a swirler and the distribution proportion of pipeline cross-section, respectively

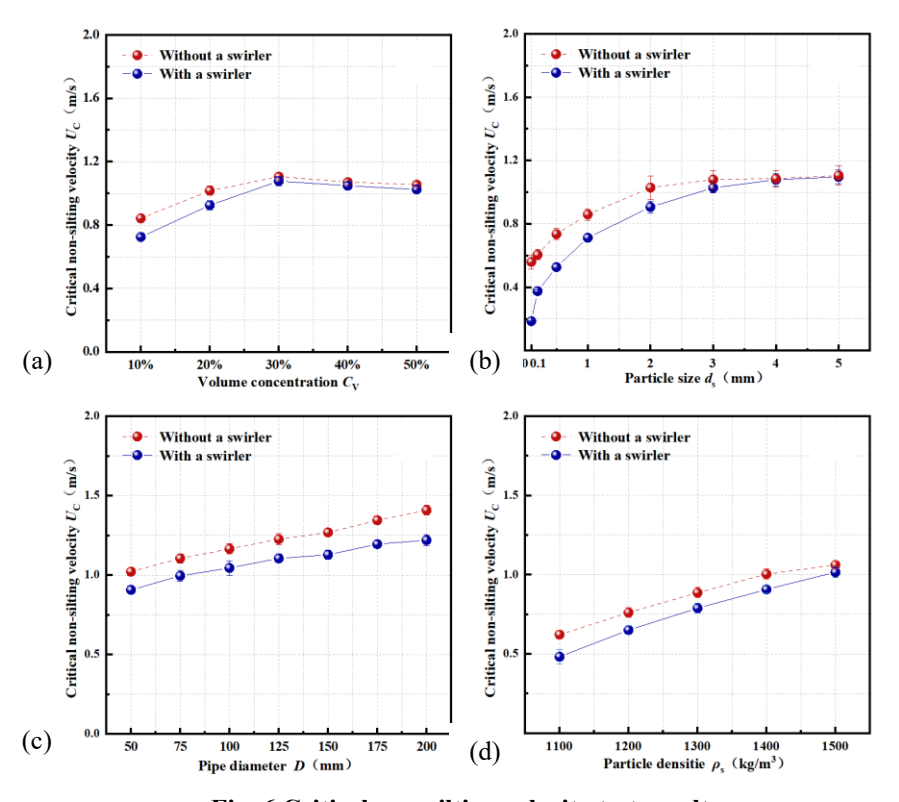


Fig. 6 Critical non-silting velocity test results

have shown that the addition of a swirler will affect the particle motion state, but no studies have shown the change law of critical non-silting flow rate after the addition of a guide vane swirler. Therefore, the critical non-silting velocity tests were carried out according to the test scheme shown in Table 2, and the test results are shown in Fig. 6.

# 3.2.1 Variation of Critical Non-silting Velocity Before Adding Swirler

As can be observed from Fig. 6(a), the critical nonsilting velocity shows a trend of first increasing significantly and then decreasing slowly with the increase in volume concentration. This phenomenon can be attributed to two main factors: on the one hand, when the volume concentration is low, increasing the slurry concentration will suppress the degree of turbulence and weaken the supporting force for particles, thus requiring a higher velocity to maintain the particles in a suspended state. On the other hand, when the concentration is high, the viscosity of the slurry increases with the concentration, making it more difficult for particles in the pipeline to settle, which in turn leads to a decrease in the critical non-silting velocity.

	Table 2	Critical	non-silting	velocity	test scheme
--	---------	----------	-------------	----------	-------------

Test numbe r	Volume concentrati on (%)	Particl e size (mm)	Pipe diamet er (mm)	Particle density (kg/m³)
a	10~50	5	50	1400
b	20	0.1~5	50	1400
c	20	5	50~200	1400
d	20	5	50	1100~150 0

As depicted in Fig. 6(b), the critical non-silting velocity increases with particle diameter. This relationship occurs because larger particles (whose density is greater than that of water) experience greater gravitational settling. Consequently, greater circumferential kinetic energy input becomes necessary to maintain suspension, thereby elevating the critical non-silting velocity.

As shown in Fig. 6(c), the critical non-silting velocity increases with the increase in particle density. The reason is similar to that when the particle diameter increases, and thus will not be reiterated herein.

Considering the difficulty of modifying the pipe diameter on the already built test bench, simulation tests are used to replace physical bench testing. The critical non-silting velocities under different pipe diameters are shown in Fig. 6(d), and the two are positively correlated. This trend can be attributed to two aspects: on the one hand, the larger the pipe diameter, the more difficult it is for the particles to return to their original positions after sedimentation, which is not conducive to particle suspension. On the other hand, the larger the diameter of the pipe, the greater the turbulent kinetic energy, which promotes the suspension of particles. Judging from the results, the former reason is dominant.

# 3.2.2 Variation of Critical Non-silting Velocity After Adding Swirler

The introduction of swirlers reduced critical nonsilting velocities across all conveying conditions compared to that without swirlers. This was because before the swirler was incorporated, the flow field within the pipeline belonged to an axial flow field. Once the swirler was added, the axial flow field was converted into a spiral flow field, while swirl-induced spiral flows impart circumferential drag forces (Fig. 7). These forces generate upward particle migration above the deposition layer and induce spiral trajectories along the pipe wall beneath it.

As demonstrated in Fig. 6(a), the critical non-silting velocity reduction was more substantial at lower concentrations. This phenomenon occurs because increased concentration requires greater circumferential velocities to reestablish non-silting conditions at constant swirler settings. Previous studies confirm that circumferential velocity is proportional to conveying velocity when the guide vane geometry remains fixed.

As evidenced in Fig. 6(b), the critical non-silting velocity reduction induced by the swirler is more pronounced for smaller particle diameters, with efficacy

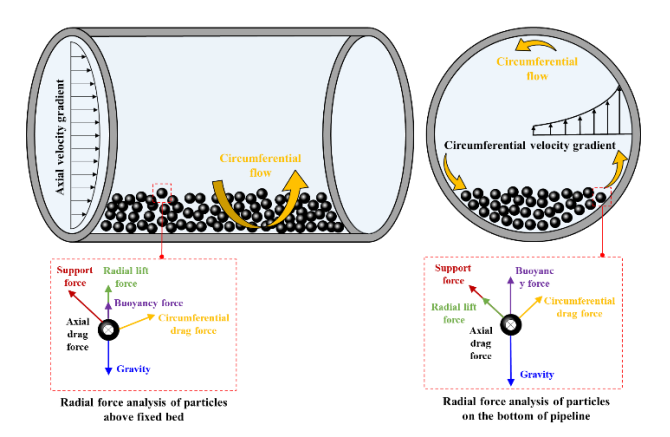


Fig. 7 Schematic diagram of particle motion analysis under the action of swirler

diminishing for larger particles. This size-dependent response aligns with Eq. (6), where particle settling velocity scales proportionally with diameter. Therefore, the smaller particles can reach a non-silting state with a lower flow velocity under the action of the swirler.

$$v_{\rm st} = \sqrt{\frac{4}{3} \frac{(\rho_{\rm s} - \rho)}{\rho} \frac{g d_{\rm max}}{C_{\rm D}}} \tag{6}$$

Equation (6) confirms that particle settling velocity scales proportionally with density. Consequently, lower-density particles exhibit greater responsiveness to swirl-induced circumferential flow, facilitating more efficient transitions from deposition to non-silting flow states, which is consistent with the result shown in Fig. 6(c).

As can be observed from Fig. 6(d), the swirler has a greater impact on the critical non-silting velocity when the pipe diameter is large. The reason is that the larger the pipe diameter, the relatively smaller the angle between the bottom wall of the pipeline and the horizontal plane, and the greater the supporting force when the particles move upward along the pipe wall. Therefore, the particles in a large-diameter pipeline are more likely to leave the bottom of the pipeline, ultimately resulting in a lower critical non-silting velocity.

### 4. CALCULATION MODEL OF CRITICAL NON-SILTING VELOCITY CONSIDERING THE SWIRL CHARACTERISTICS

The incorporation of the swirler transforms the axial flow field in the conveying pipeline into a spiral flow field, which is more conducive to particle suspension. The critical non-silting velocity is defined as the flow velocity at which all particles that were stationary and deposited at the bottom of the conveying pipeline start to move forward. Therefore, the critical non-silting velocity in the spiral flow field of the pipeline must take the influence of swirling flow characteristics into account. Therefore, by analyzing the functional relationship between the critical non-silting velocity and its influencing factors under the action of the swirler, a calculation model of the critical non-silting velocity considering the characteristics of the swirling flow is established in the following.

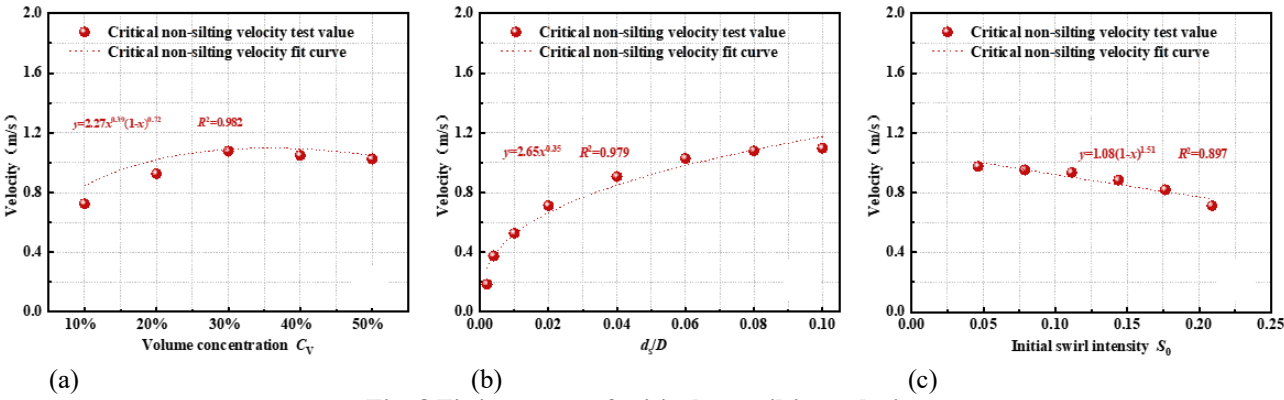


Fig. 8 Fitting curve of critical non-silting velocity

### 4.1 Functional Relationship between Critical Nonsilting Velocity and Its Influencing Factors

As can be seen from the above content, the critical non-silting velocity  $U_{\rm C}$  exhibits strong functional dependencies on volumetric concentration  $C_{\rm V}$ , particle diameter ds, particle density  $\rho_{\rm s}$ , and pipe inner diameter D. There are commonalities in the structural forms of the critical non-silting velocity calculation models proposed by different scholars, as shown in Eq. (7). Combined with the research results on the influence laws of the critical non-silting velocity, the dimensional analysis method is employed to analyze the functional relationships among the volume concentration, particle diameter, and critical non-silting velocity under the action of the swirling device. Meanwhile, taking into account the impact of the swirling device on the critical non-silting velocity, the critical non-silting velocity calculation model is modified.

$$U_{\rm c} \propto \sqrt{gD \frac{(\rho_s - \rho)}{\rho}} \tag{7}$$

Volumetric concentration exerts antagonistic effects on critical non-silting velocity: on the one hand, the increase in volume concentration leads to an increase in slurry viscosity, and the particles are more difficult to settle. On the other hand, the increase in volume concentration can inhibit the turbulence intensity, which is not conducive to particle suspension. We proposed Eq. (8) to describe these two effects. The fitting results are shown in Fig. 8(a), and the final functional relationship is shown in Eq. (9).

$$v = a \cdot x^b \cdot (1 - x)^c \tag{8}$$

where, a, b and c are undetermined coefficients.

$$U_{\rm C} \propto f \left\lceil C_{\rm V}^{0.39} \cdot (1 - C_{\rm V})^{0.72} \right\rceil \tag{9}$$

The critical non-silting velocity scales proportionally with both particle diameter and pipe diameter. We select the dimensionless diameter ratio  $d_s/D$ , as the governing parameter. The fitted functional relationship (Fig. 8b) yields the empirical correlation expressed in Eq. (10).

$$U_{\rm C} \propto f \left[ \left( \frac{d_{\rm s}}{D} \right)^{0.35} \right] \tag{10}$$

While swirlers universally reduce critical non-silting velocity by mitigating particle sedimentation under identical conveying conditions, the quantitative relationship between swirl characteristics and critical non-silting velocity remains empirically unquantified. To resolve this, we systematically measured critical velocity variation against initial swirl intensity  $S_0$ , as shown in Fig. 8(c), where  $S_0$  is defined by Eq. (11). The resulting functional correlation between initial swirl intensity and critical velocity is established in Eq. (12).

$$S = S_0 e^{-\beta (Z_{SD}/D)} \tag{11}$$

$$U_{\rm C} \propto f \left[ \left( 1 - S_0 \right)^{1.51} \right] \tag{12}$$

Where,  $S_0$  is the initial swirl intensity.  $\beta$  is the decay rate of swirl intensity, and its value is related to the guide vane parameters of the swirler and the conveying velocity.

# 4.2 Construction and Modification of Calculation Model of Critical Non-silting Velocity

Synthesizing Eqs. (9), (10), and (12) yields a comprehensive critical non-silting velocity model incorporating swirl characteristics, as formalized in Eq. (13).

$$U_{\rm C} = K \sqrt{gD \frac{(\rho_s - \rho_l)}{\rho_l}} C_{\rm V}^{0.39}$$

$$(1 - C_{\rm V})^{0.72} \left(\frac{d_{\rm s}}{D}\right)^{0.35} (1 - S_0)^{1.51}$$
(13)

The spiral flow induced by the swirler undergoes progressive attenuation per Eq. (11). This decay implies that beyond sufficient downstream distance, the flow's anti-sedimentation effect diminishes, reverting to baseline axial transport characteristics. We establish the distance-dependent attenuation function in Eq. (14) and incorporate it into the critical non-silting velocity model's swirl parameterization, yielding the position-corrected formulation in Eq. (15).

$$\chi(Z_{\rm sd}) = e^{-\beta(Z_{\rm sd}/D)} \tag{14}$$

$$U_{\rm C} = K \sqrt{gD \frac{(\rho_{\rm s} - \rho_{l})}{\rho_{l}}} C_{\rm V}^{0.39} (1 - C_{\rm V})^{0.72}$$

$$\left(\frac{d_{\rm s}}{D}\right)^{0.35} \left(1 - S_{\rm 0} \cdot \chi(Z_{\rm sd})\right)^{1.51}$$
(15)

Table 3 Bench verification test scheme for calculating model of critical non-silting velocity

Test group	$C_{ m V}$	$d_{\rm s}$ / mm	$ ho_{ m s}$ / kg·m <sup>-3</sup>
1	20%	0.2	1100
2	20%	0.5	1500
3	20%	5	1300
4	35%	0.2	1500
5	35%	0.5	1300
6	35%	5	1100
7	50%	0.2	1300
8	50%	0.5	1100
9	50%	5	1500

Based on empirical data from Fig. 6, the calibration constant K in Eq. (15) was determined through non-intercept linear regression analysis using SPSS software. Values of particle concentration, diameter, density, and pipe diameter across all experimental conditions were substituted into Eq. (15). A regression-through-the-origin model (no intercept) was implemented, yielding a fitted value of K=15.54 (R<sup>2</sup> = 0.997, Sig. value is 5.78E-36).

To verify the accuracy of the established critical nonsilting velocity model, a bench verification test was conducted by employing the established critical nonsilting velocity test apparatus following the test scheme for the calculation model of the critical non-silting velocity presented in Table 3. Figure 9 illustrates the particle motion states corresponding to the various groups in the critical non-silting velocity verification test.

It can be observed that before the attainment of the critical non-silting velocity by the conveying velocity, particles were deposited at the bottom of the pipeline in each test group (as indicated by the yellow box in Fig. 9). Once the flow velocity was increased to the critical non-silting velocity, all particles moved forward along with the flow field. Among these, in Fig. 9 (a), (d), and (g), the particle diameter under the corresponding working conditions is 0.2 mm. Due to the relatively small particle diameter, when the non-silting flow commences, the slurry within the conveying pipeline becomes more turbid compared to the situation where the particle size is larger.

Comparative analysis in Fig. 10 demonstrates that the critical non-silting velocity model proposed in this study maintains alignment with other scholars' models in overall trend while achieving superior accuracy. Our model exhibits significantly reduced deviation from experimental values, with a mean absolute error of 9.10% and maximum error of 14.08%.

Furthermore, Test Groups 1, 2, 4, 5, 7, and 8 exhibit significantly smaller deviations between experimental values and our model predictions compared to other scholars' models. Analysis of corresponding transport parameters reveals these groups share the distinctive feature of fine particle sizes (0.2-0.5 mm). This aligns with the established particle diameter dependence: swirl generators preferentially modify sedimentation dynamics of fine particles through enhanced rotational coupling, substantially reducing their critical non-silting velocity. The model's superior performance across these conditions confirms its efficacy in predicting critical non-silting

velocities for swirler-induced helical flows in slurry pipelines.

### 5. CONCLUSIONS

This paper proposes a measure of installing a swirler to solve the problem of particle sedimentation in horizontal conveying pipelines. Through simulation and bench tests, the following conclusions have been obtained.

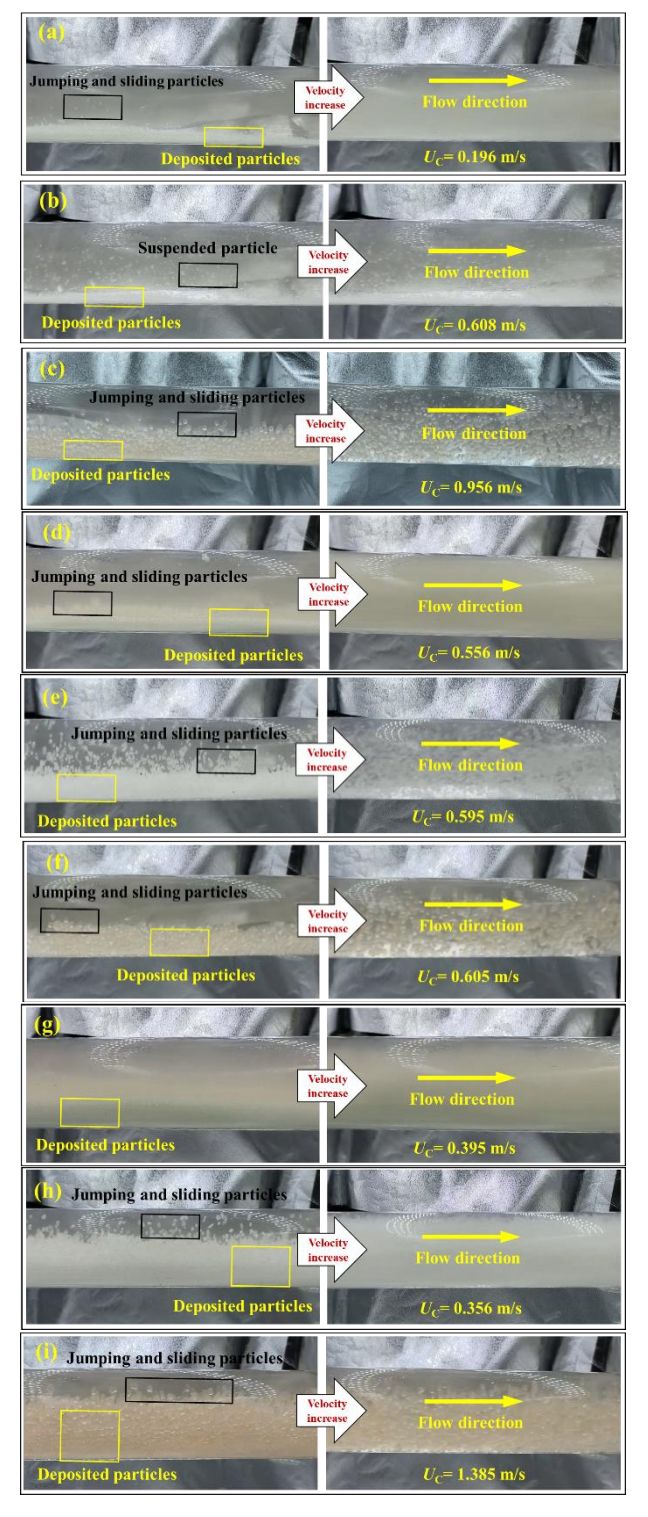


Fig. 9 Particle motion state of critical non-silting velocity verification test. a-i represents test group number 1-9

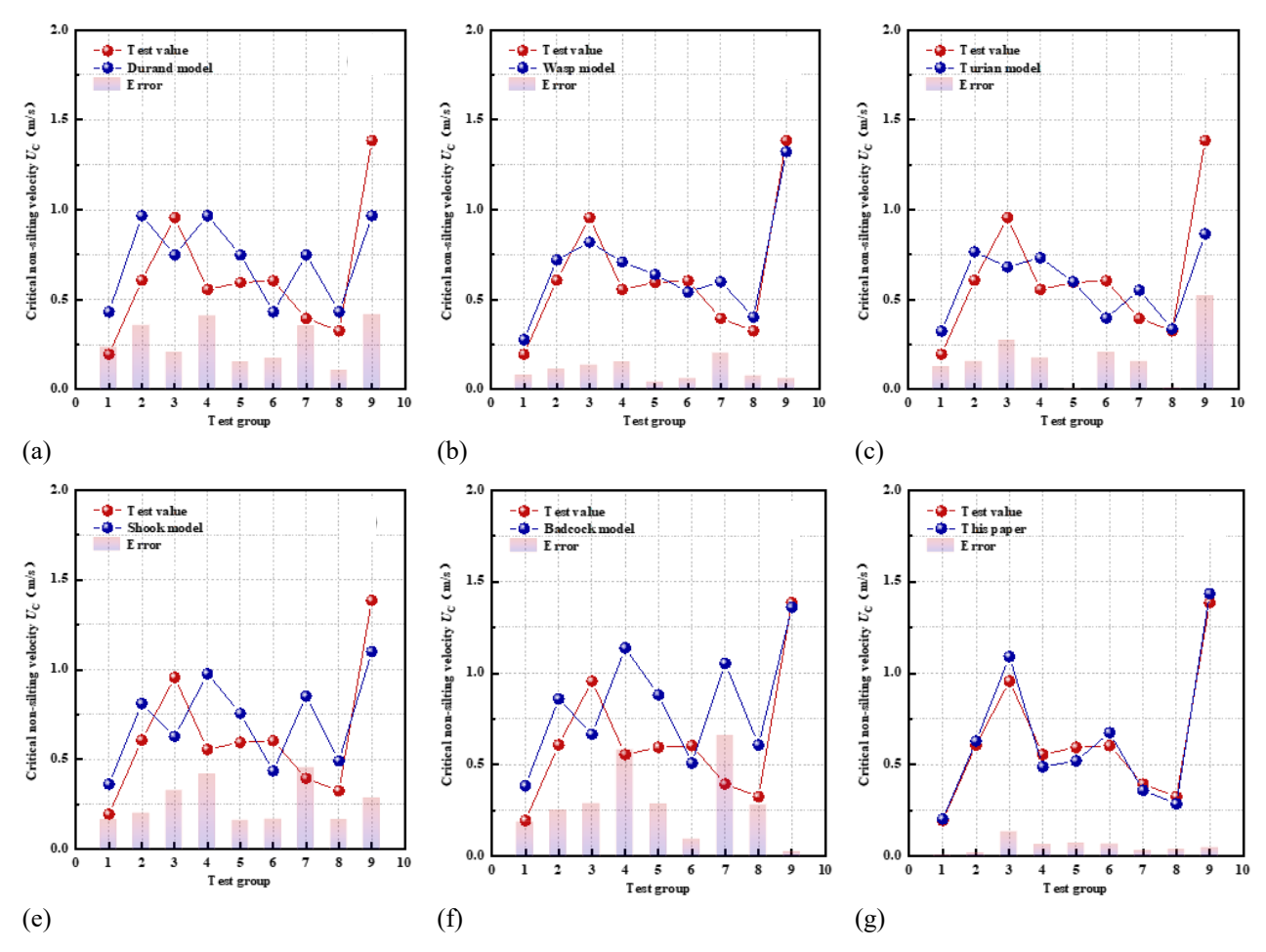


Fig. 10 Comparison of calculated model and test values. a-g is the calculation model of Durand, Wasp, Turian, Shook, Badcock, and this paper respectively

1) Swirlers transform axial flow into spiral flow fields within pipelines. The drag force of the circumferential water flow causes the particles to rise and move along the pipe wall. The pipe wall provides a supporting force, and the circumferential flow velocity can lift the particles that may settle again, making the particles more likely to be suspended. Consequently, the critical non-silting velocity is reduced.

2) The critical non-silting velocity exhibits a trend of initially increasing and then decreasing with the increase in volume concentration, while it tends to increase with larger particle diameters, higher particle densities, and larger pipeline diameters. Swirler efficacy in reducing critical non-silting velocity is maximized under lowconcentration conditions with small particle diameters and low-density particles. This phenomenon stems from the enhanced hydrodynamic responsiveness of smaller or lower-density particles to circumferential flows, where reduced particle inertia facilitates motion-state modification under rotational forcing. In larger-diameter pipes, reduced wall curvature decreases the effective gravitational force component normal to the surface. This geometric configuration enhances normal force efficacy during particle uplift, significantly facilitating detachment from deposition zones and thereby reducing critical nonsilting velocity.

3) A predictive model for critical non-silting velocity, incorporating swirl flow characteristics and augmented with helical flow decay dynamics, has been developed. This model demonstrates exceptional agreement with experimental data, particularly for fine-particle slurries, achieving a mean absolute error of 9.10% and a maximum error of 14.08%.

### **ACKNOWLEDGEMENTS**

This work was supported in China by the National Natural Science Foundation of China (Grant No. 52404165), the Natural Science Foundation of the Jiangsu Higher Education Institutions (Grant No. 25KJD440001), and the Xuzhou Science and Technology Program (Grant No. KC2025012).

### **CONFLICT OF INTEREST**

Authors declare that they have no conflicts to disclose.

### **AUTHORS CONTRIBUTION**

Shaodi Zhao: Writing-riginal draft, Writing-review & editing. Jiusheng Bao: Conceptualization. Jinjie Ji: Investigation. Xing Zhang: Validation. Yansong Ma:

Visualization. Yan Yin: Methodology. Yuhang Liu: Software.

#### REFERENCES

- Bao, J. S., Zhao, S. D., Wang, Z. B., Ge, S. R., Yin, Y., Huang, C. G., & Zhou, H. (2022). A deep coal fluidized pipeline transportation system. [ZL202110715365.2]. China National Intellectual **Property** Administration, 2022-02-18. https://kns.cnki.net/kcms2/article/abstract?v=o8vM LOX1CKv9b1WdRNtmgyCB-yPmJ7xAMihYJ72ynZ4mX2FQs8zsrYs5QHzbKkEP1U-qeAHgJZIWCyQ1DC DfkKwfjjEpYqH2JOkCjnmbxSF DnddFqWEMkuzZCwleRBGtGJtVocrNHt G3Er38 v359ncjOA9KAe0RG261CIwLW2tercU9l4Q==&u niplatform=NZKPT&language=CHS
- Bao, J. S., Zhao, S. D., Yin, Y., Wang, Z. B., Liu, S., & Ge, S. R. (2025). Nonsilting transport characteristics of coal slurry in a deep underground fluidization conveying pipeline under the action of a guide vane swirler. *Deep Underground Science and Engineering*, 1-17. https://doi.org/10.1002/dug2.70026
- Baria, S, & Saad, I. (2013). CFD modelling of the effect of guide vane swirl and tumble device to generate better in-cylinder air flow in a CI engine fuelled by biodiesel. *Computers & Fluids*, 84, 262-69. https://doi.org/10.1016/j.compfluid.2013.06.011
- Chen, S. D., Tang, D. Z., Hou, W., Li, Y. Z., Tao, S., Xu, H., Li, S., Tang, S. L., Pu, Y. F., & Zhang, B. (2023). Geological particularity and reservoir engineering response of deep coalbed methane. *Acta Petrolei Sinica*, 44(11), 1993-2006. https://doi.org/10.7623/syxb202311018.
- Das, D., Das, S. K., Parhi, P. K., Dan, A. K., Mishra, S., & Misra, P. K. (2021). Green strategies in formulating, stabilizing and pipeline transportation of coal water slurry in the framework of WATER-ENERGY NEXUS: A state of the art review. *Energy Nexus*, 4, 100025. <a href="https://doi.org/10.1016/j.nexus.2021.100025">https://doi.org/10.1016/j.nexus.2021.100025</a>
- Das, S. N., Biswal, S. K., & Mohapatra, R. K. (2020). Recent advances on stabilization and rheological behaviour of iron ore slurry for economic pipeline transportation. *Materials Today: Proceedings*, *33*, 5093-5097. https://doi.org/10.1016/j.matpr.2020.02.851.
- Durand, R. (1952). The hydraulic transportation of coal and other materials in pipes. London: College National Board.
- Galy, B., & Giraud, L. (2023). Risk mitigation strategies for automated current and future mine hoists. *Safety Science*, 167, 106267. <a href="https://doi.org/10.1016/j.ssci.2023.106267">https://doi.org/10.1016/j.ssci.2023.106267</a>
- Gao, J., Hao, X. D., Wang, L., & Wang, P. (2016). Resistance characteristics of coal slime in pipe flow at high pressure. *International Journal of Chemical*

- *Reactor Engineering*, *14*(1), 299-307. https://doi.org/10.1515/ijcre-2015-0076
- Kim, I., Kim, J., Choe, Y., Ryu, K., Cha, J., & Ri, J. (2023). Effect of vane angle on combustion characteristics of premixed H2/air in swirl microcombustors with straight vane or twisted vane. *Applied Thermal Engineering*, 228, 120528. <a href="https://doi.org/10.1016/j.applthermaleng.2023.1205">https://doi.org/10.1016/j.applthermaleng.2023.1205</a>
- Li, X. Y. (2021). Dewatering technology and system configuration at terminal of shenwei high concentration coal slurry piping line. *Coal Technology*, 40(5), 193-195. https://doi.org/10.13301/j.cnki.ct.2021.05.053.
- Li, Y. G., Pang, Y. Q., Song, X. T., Jia, X. M., Lu, Y. F., Sun, X. H., & Zhang, X. L. (2021). Influence of setting angle for guide bar on velocity characteristics of spiral flow in cross-sections between piped carriages. *Transactions of the Chinese Society of Agricultural Engineering*, 37(5), 87-94. <a href="https://doi.org/10.11975/j.issn.1002-6819.2021.05.010">https://doi.org/10.11975/j.issn.1002-6819.2021.05.010</a>
- Li, Y., Liu, D. X., Cui, B. L., Lin, Z., Zheng, Y. H., & Ishnazarov, O. (2024). Studying particle transport characteristics in centrifugal pumps under external vibration using CFD-DEM simulation. *Ocean Engineering*, 301, 117538. https://doi.org/10.1016/j.oceaneng.2024.117538
- Lu, Y. (2020). Application status and development direction of coal slurry pipeline transportation technology. www.gdchem.com, 47(10), 67-68. CNKI:SUN:GDHG.0.2020-10-032
- Ma, Y., Chen, J. Q., Men, Z. M., Ruan, Z. Y., Zou, D. Z., Zuo, H. Q., & Han, W. L. (2017). Optimization of coal pipeline transportation parameters. *Coal Engineering*, 49(5), 107-111. <a href="https://doi.org/10.11799/ce201705032">https://doi.org/10.11799/ce201705032</a>
- Saad, I., & Baria, S. (2014). Guide vane swirl and tumble device to improve in-cylinder air flow of CI engine using vegetable oil. *Procedia Engineering*, 90, 425-30. <a href="https://doi.org/10.1016/j.proeng.2014.11.872">https://doi.org/10.1016/j.proeng.2014.11.872</a>
- Singh, M. K., Kumar, S., & Ratha, D. (2020). Computational analysis on disposal of coal slurry at high solid concentrations through slurry pipeline. *International Journal of Coal Preparation and Utilization*, 40(2), 116-130. https://doi.org/10.1080/19392699.2017.1346632
- Singh, M. K., Kumar, S., Ratha, D., & Kaur, H. (2019). Improvement in head loss characteristics of fine particulate coal water suspension with addition of coarser particulate. *International Journal of Coal Preparation and Utilization*, 42(3), 305-314. https://doi.org/10.1080/19392699.2019.1600512
- Singh, R. P., Mallick, M., & Verma M. K. (2016). Studies on failure behaviour of wire rope used in underground coal mines. *Engineering Failure Analysis*, 70, 290-304. https://doi.org/10.1016/j.engfailanal.2016.09.002

- Sun, X. H., Yan, Q. F., & Li, Y. Y. (2012). Study on Hydraulic Characteristics of Pipe Helical Flow Transportation. Beijing: China Water and Power Press.
- Wang, D. G., Zhang, J., Ge, S. R., Zhang, D. K., & Shi, G. Y. (2019). Mechanical behavior of hoisting rope in 2 km ultra deep coal mine. *Engineering Failure Analysis*, 106, 104185. https://doi.org/10.1016/j.engfailanal.2019.104185
- Xie, H. P., Gao, F., Ju, Y., Zhang, R., Gao, M. Z., & Deng, J. H. (2017a). Novel idea and disruptive technologies for the exploration and research of deep earth. Advanced Engineering Sciences 49(1), 1-8. https://doi.org/10.15961/j.jsuese.2017.01.001
- Xie, H. P., Gao, F., Ju, Y., Ge, S. R., Wang, G. F., Zhang, R., Gao, M. Z., Wu, G., & Liu, J. Z. (2017b). Theoretical and technological conception of the fluidization mining for deep coal resources. *Journal of China Coal Society*, 42(3), 547-56. https://doi.org/10.13225/j.cnki.jccs.2017.0299
- Xie, H. P., Ju Y., Ren S. H., Gao F., Liu J., & Zhu Y. (2019). Theoretical and technological exploration of deep in situ fluidized coal mining. *Frontiers in Energy*, 13(4), 603-611. <a href="http://dx.doi.org/10.1007/s11708-019-0643-x">http://dx.doi.org/10.1007/s11708-019-0643-x</a>
- Xie, H. P., Ju, Y., Gao, M. Z., Gao, F., Liu, J. Z., Ren, H. W., & Ge, S. R. (2018). Theories and technologies for in-situ fluidized mining of deep underground coal resources. *Journal of China Coal Society*, 43(5), 1210-1219.
  - http://dx.doi.org/10.13225/j.cnki.jccs.2018.0519

- Zhang, Q. H., Wang, X. R., & Yuan, L. (2023). Development of a multi-field coupled numerical simulation program for underground coal gasification and multi-field evolution laws. *Journal of China Coal Society*, 48(6), 2506-2518. <a href="http://dx.doi.org/10.13225/j.cnki.jccs.xh22.1670">http://dx.doi.org/10.13225/j.cnki.jccs.xh22.1670</a>
- Zhao, S. D. (2024). Research on slurry non-silting characteristics and elbow wear rule of deep coal fluidized pipeline lifting system (Doctoral Dissertation). China University of Mining and Technology, Xuzhou. <a href="https://doi.org/10.27623/d.cnki.gzkyu.2024.000222">https://doi.org/10.27623/d.cnki.gzkyu.2024.000222</a>
- Zhao, S. D., Bao, J. S., Ge, S. R., Wang, Z. B., Yin, Y., & Huang, C. G. (2024). Influence and optimization of swirler parameters on elbow wear of deep coal fluidization pipeline transportation system. *Friction*, *12*, 1408-1433. <a href="https://doi.org/10.1007/s40544-023-0781-3">https://doi.org/10.1007/s40544-023-0781-3</a>
- Zhao, S. D., Bao, J. S., Ge, S. R., Wang, Z. B., Yin, Y., & Li Y. F. (2023). Influence of solid-liquid two-phase flow conveying parameters on the elbow wear with and without the swirler. *Tribology International*, 186, 108635.
  - https://doi.org/10.1016/j.triboint.2023.108635.
- Zhou, J. W., Du, C. L., Liu, S. Y., & Liu, Y. (2016). Comparison of three types of swirling generators in coarse particle pneumatic conveying using CFD-DEM simulation. *Powder Technology*, 301, 1309-1320.

http://dx.doi.org/10.1016/j.powtec.2016.07.047